

Matrix Vesicles and Focal Proteoglycan Aggregates Are the Nucleation Sites Revealed by the Lanthanum Incubation Method: A Correlated Study on the Hypertrophic Zone of the Rat Epiphyseal Cartilage

S. Gomez,¹ J. M. Lopez-Cepero,¹ G. Silvestrini,² P. Mocetti,² E. Bonucci²

¹Department of Pathological Anatomy, Faculty of Medicine, University of Cadiz, Spain

²Department of Experimental Medicine and Pathology, Section of Pathological Anatomy, Policlinico Umberto I, Viale Regina Elena 324, University La Sapienza, 00161 Rome, Italy

Received: 27 April 1995 / Accepted: 20 October 1995

Abstract. Correlated studies were performed with light and electron microscopy, and backscattered electron image in conjunction with X-ray microanalysis, of lanthanum-incubated epiphyseal cartilage of the young rat. The hallmark of this procedure is the appearance of LaP electron-dense deposits (not present in control sections) in precise sites of the hypertrophic zone. The ultrastructural study revealed a dual nature of these sites: “dense matrix vesicles” and “focal filament aggregates.” The dense matrix vesicles are a specific type of matrix vesicle with the intrinsic capacity of precipitating LaP mineral, as soon as they originate from the hypertrophic chondrocytes. Furthermore, the matrix vesicles were found to be heterogeneous because lanthanum-devoid, “light matrix vesicles” were also present. The focal filament aggregates, which were not recognized in unstained sections and in controls, are apparently focal concentrations of proteoglycans with high lanthanum binding capacity, although the presence in them of other components (e.g., type X collagen, C-propeptide of type II collagen) cannot be excluded. They were in close connection with the light matrix vesicles in the upper hypertrophic zone, and were loaded with a variable quantity of LaP irregular electron-dense deposits in the lower hypertrophic zone. These irregular deposits are similar to, but distinct from, calcification nodules. The lanthanum incubation method indirectly detects the matrix Ca-binding components (which bind La ions), and the calcification initiation sites (which precipitate a LaP-mineral phase). A sequence is proposed of successive steps of LaP nucleation within the focal filament aggregates, which possibly mimics calcium phosphate deposition. Such a sequence seems to require the participation not only of dense matrix vesicles, but also of the filamentous components of the focal aggregates, possibly together with the activity of alkaline phosphatase.

Key words: Lanthanum — Cartilage — Calcification — Matrix vesicles — Proteoglycans.

The lanthanum incubation method is based on the premise that La^{3+} and Ca^{2+} have the same ionic radius, but La^{3+} has a higher valence and is more tightly bound to organic sub-

strates than Ca^{2+} ; the expectation is that La^{3+} binds to the same matrix components as Ca^{2+} , but less reversibly, and it remains so during specimen preparation and electron microscope examination. The lanthanum incubation method was proposed by Morris and Appleton [1] to study the calcium binding sites in the cartilage matrix as an alternative method to the potassium-pyrosulfate-osmium ultrahistochemistry. The lanthanum incubation method was first applied to normal and rachitic condylar cartilage. The electron microscope results showed the presence of electron-dense deposits located around the hypertrophic chondrocyte peripheral membrane, as well as in the extracellular matrix. Rachitic condylar cartilage showed marked reduction in the quantity of electron-dense deposits, but a restoration followed in rats treated with vitamin D.

The electron-dense deposits have a distribution tendency similar to that of the calcification nodules, and consist of needle- and filament-like structures similar to apatite crystallites, so that they can be hardly differentiated from areas of early calcification. For this reason, further electron microscopic analysis was carried out on lanthanum incubated epiphyseal cartilage of the young rat. The principal aim was to identify the nature of the electron-dense deposits as well as the related matrix components. In the present study the lanthanum incubation method proved to be a sensitive method for detecting the calcium binding sites and the calcification initiation sites of the hypertrophic zone.

Materials and Methods

Light and Electron Microscopy

Small and thin ($1 \times 2 \times 2$ mm) fragments of metatarsal and tibial epiphyseal cartilage of 8-day-old Wistar rats and tibial epiphyseal growth plate of 15- and 21-day-old Wistar rats were incubated in a solution containing 15 mM (0.557 g/100 ml) of lanthanum chloride, fixed and processed as reported [1]. Control samples were treated without lanthanum chloride. Semithin sections were examined under the light microscope after (1) staining with toluidine blue-pyronine G, (2) staining with azur II-methylene blue, (3) using the von Kossa method, (4) impregnation with ammoniacal silver at 55°C, until the sections take on a brown color, and (5) decalcification by floatation for 10 minutes on 10% EDTA or 2% formic acid, followed by toluidine blue-pyronine G staining or ammoniacal silver impregnation.

The ultrastructural study was performed on the uncalcified (i.e., von Kossa negative) hypertrophic zone of the epiphyseal cartilage.

To select this zone, the blocks were trimmed under microscopic control until the zone of calcifying cartilage and chondrocyte disintegration was present only at a very marginal portion of the specimen in von Kossa-stained sections. The selected zone was arbitrarily divided into three parts: (1) the upper hypertrophic zone (i.e., the part approaching the cartilage maturation zone); (2) the lower hypertrophic zone (i.e., the part with hypertrophic chondrocytes); (3) and the lowest hypertrophic zone (i.e., the very marginal portion where degenerated and fragmented chondrocytes and von Kossa-positive granules could be found).

In the first place, "unstained" ultrathin sections were mounted on aluminium grids and examined under a JEOL-JEM 1200 microscope (Jeol L.T.D., Tokyo, Japan) equipped with a LINK LZ5 X-ray microanalysis system to search for lanthanum precipitates and to describe their distribution [1]. Then, ultrathin sections were examined under a CM10 Philips TEM (Philips Export B.V., Eindhoven, The Netherlands) after using the following procedures: (1) decalcification by flotation on EDTA or formic acid; (2) staining with uranyl acetate and lead citrate (U/Pb); (3) staining with 2% phosphotungstic acid in aqueous solution (PTA); (4) decalcification by flotation on EDTA or formic acid followed by uranyl acetate and lead citrate staining (post-embedding decalcification and staining; PEDS method [2]).

Correlated Backscattered Electron Image in Conjunction with Mapping X-ray Microanalysis

Correlated analyses were conducted in a JEOL-JSM820 SEM (scanning electron microscope) equipped with a Link AN 10/85 energy dispersive X-ray analytical system and a solid state annular backscattered electron image detector. The SEM was operated at 20 kV. The backscattered electron image (BSE) and X-ray microanalysis were performed on the carbon-coated block surface of the La-incubated cartilage previously used for ultrastructural study. These block surfaces can be considered as flat surfaced bulk samples suitable for BSE-SEM, X-ray microanalysis, and correlated studies [3]. The spatial X-ray resolution obtained was about 1 μm . The block surface was examined first with BSE-SEM to recognize the chondrocyte morphology and distribution of lanthanum focal deposits. Then selected scanned fields were analyzed. Characteristic X-rays of elements were first qualitatively identified and their net peak intensities were evaluated. A simultaneous mapping X-ray microanalysis was then recorded by fixing six windows to identify, respectively, phosphorus (P = 1.920–2.080 kV), sulphur (S = 2.240–2.360 kV), calcium (Ca = 3.640–3.740 kV), lanthanum (La = 4.560–4.720 kV), and two background sectors (BG1 = 3.080–3.460 kV; BG2 = 3.940–4.360 kV).

Results

Light Microscope Examination

After La incubation, the morphology of the epiphyseal chondrocytes appeared well preserved. The intriguing finding was the appearance in the hypertrophic zone, but not in the proliferative zone, of stainable deposits located in the interterritorial matrix and around the chondrocyte peripheral membrane with a typical distribution.

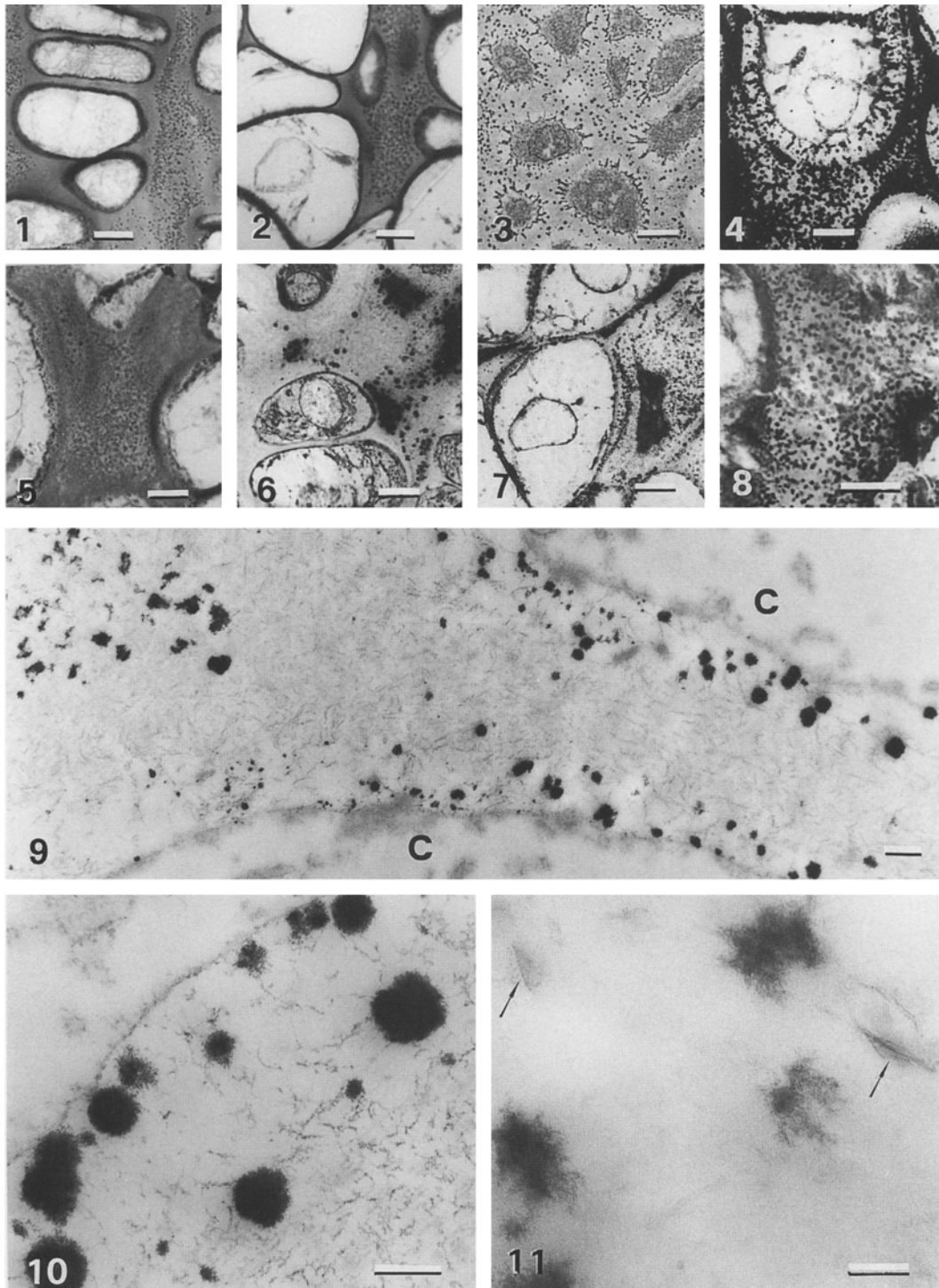
In the interterritorial matrix of the hypertrophic zone the deposits were numerous, small dots (about 1–2 μm in diameter) deeply stained by toluidine blue (Figs. 1, 2), methylene blue, or ammoniacal silver impregnation (Figs. 3, 4), even after decalcification with EDTA or formic acid (Figs. 5, 6, 7). The dots were abundant and bigger in the lowest zone, where they were heavily impregnated by silver. Moreover, the small dots present in upper and lower hypertrophic zones were all von Kossa negative, whereas part of those of the lowest hypertrophic zone were positive (i.e., they were calcification nodules; Fig. 8). In the control cartilage, the dots were restricted to the lowest zone of the hypertrophic cartilage.

The deposits around the chondrocyte peripheral membrane were better appreciated by ammoniacal silver impregnation and were not present in the controls. In the upper hypertrophic zone, the deposits outlined the peripheral membrane of the chondrocytes (Fig. 3). In the lower hypertrophic zone, they appeared as distinct dots in close contact with the peripheral membrane and capsular material (Figs. 4, 7). In the lowest zone, numerous von Kossa-negative dots, visible after toluidine blue staining (Fig. 5), were present around the chondrocyte peripheral membrane.

Transmission Electron Microscope Examination

On initial examination, electron microscopy of the "unstained" sections showed the presence in definite sites of electron-dense deposits. A preliminary control X-ray microanalysis showed that these deposits contained lanthanum and phosphorus. They were found in territorial and interterritorial matrix of the lower hypertrophic zone (Fig. 9),

- Fig. 1.** Upper hypertrophic zone: numerous deeply stained dots are present in interterritorial matrix. Toluidine blue-pyronine G; bar = 10 μm .
- Fig. 2.** Lower hypertrophic zone: dots present in interterritorial matrix. Toluidine blue-pyronine G; bar = 10 μm .
- Fig. 3.** Maturing zone: linear deposits around the chondrocyte membrane and dots in interterritorial matrix. Ammoniacal silver impregnation; bar = 10 μm .
- Fig. 4.** Lowest hypertrophic zone: deposits are abundant around the chondrocyte membrane, and in territorial and interterritorial matrix. Ammoniacal silver impregnation; bar = 10 μm .
- Fig. 5.** EDTA-decalcified lowest hypertrophic zone: deposits are visible around the chondrocyte membrane and in territorial and interterritorial matrix, in spite of section decalcification. EDTA/toluidine blue-pyronine G; bar = 10 μm .
- Fig. 6.** EDTA-decalcified upper hypertrophic zone: clusters of deposits are seen in interterritorial matrix. EDTA/ammoniacal silver impregnation; bar = 10 μm .
- Fig. 7.** EDTA-decalcified lower hypertrophic zone: separate deposits around the chondrocyte membrane. EDTA/ammoniacal silver impregnation; bar = 10 μm .
- Fig. 8.** Lowest hypertrophic zone: von Kossa-positive (below) and von Kossa-negative (above) dots are present in the same area of interterritorial matrix. Von Kossa/toluidine blue-pyronine G; bar = 10 μm .
- Fig. 9.** Lower hypertrophic zone: electron-dense deposits are present in both territorial and interterritorial matrix. C: chondrocyte lacunae; unstained, $\times 6610$; bar = 1 μm .
- Fig. 10.** Lower hypertrophic zone: a small portion of hypertrophic chondrocyte is visible on the upper left; the electron-dense deposits are located close to, and in the proximity of, the chondrocyte peripheral membrane. Their roundish shape suggests that they probably correspond to dense MVs, as shown in Figures 12 and 13. Compare with Figure 11. U/Pb, $\times 21,000$; bar = 0.5 μm .
- Fig. 11.** Lower hypertrophic zone: small, roundish or irregular, electron-dense deposits ("irregular electron-dense deposits"), and less electron-dense, needle-shaped deposits, probably corresponding to apatite crystallites (arrows), are visible in interterritorial matrix. Compare with Figure 10. Unstained, $\times 50,000$ bar = 0.25 μm .



were completely removed by EDTA or formic acid treatment, and were heavily stained by U/Pb.

A close observation of these deposits revealed two distinct morphologies: some were globular (Fig. 10), others had an irregular shape (Fig. 11; see below). After examining PTA or PEDS-stained sections, we realized that the globular deposits were matrix vesicles (MVs). In fact, they appeared as globular (80–170 nm in diameter) structures (Fig. 12)

surrounded by a dense, membrane-like peripheral border (20–30 nm thick) (Fig. 13). Their matrix was homogeneous and electron-dense, thus they are called “dense” MVs. They were often in contact with collagen fibrils and were sometimes connected to the extremity of a cellular process (Figs. 12, 13). The dense MVs were abundant at the pericellular rim and in the territorial matrix of hypertrophic chondrocytes. In interterritorial matrix they were found both

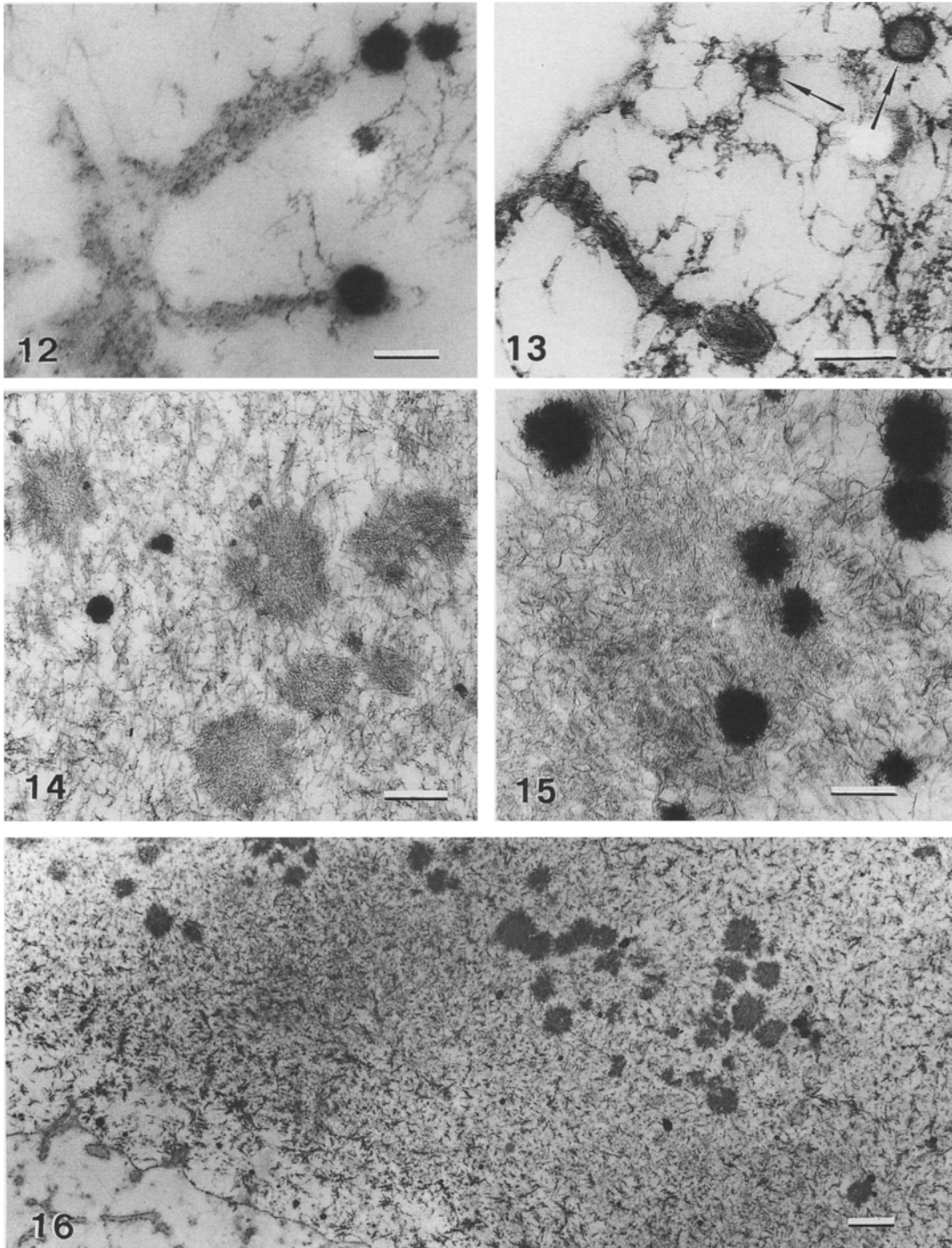


Fig. 12. Upper hypertrophic zone: a very small portion of a hypertrophic chondrocyte, and two cell processes are visible; globular electron-dense deposits, probably corresponding to dense MVs, are connected to the extremity of the cell processes. U/Pb, $\times 21,000$; bar = $0.5 \mu\text{m}$.

Fig. 13. Upper hypertrophic zone: section decalcified by flotation on formic acid; a dense MV is located at the tip of a cell process; other dense MVs (arrows) show a membrane-like peripheral border. PEDS method: formic acid-U/Pb, $\times 28,500$, bar = $0.5 \mu\text{m}$.

Fig. 14. Upper hypertrophic zone: two dense MVs, easily recognizable because of their high electron density, and six focal filament aggregates are present in this portion of the interterritorial matrix; the focal aggregates appear as small, roundish clusters of filaments which mask the other structures of the matrix. U/Pb, $\times 11,500$; bar = $1 \mu\text{m}$.

Fig. 15. Lower hypertrophic zone: seven dense MVs are visible; three of them are located over a focal filament aggregate, two are at its border, and two (upper right corner) are in the matrix. U/Pb, $\times 21,000$; bar = $0.5 \mu\text{m}$.

Fig. 16. Upper hypertrophic zone: several focal filament aggregates are visible in interterritorial matrix; they appear as roundish, moderately electron-dense structures. Part of a chondrocyte on lower left. U/Pb, $\times 3,900$; bar = $2 \mu\text{m}$.

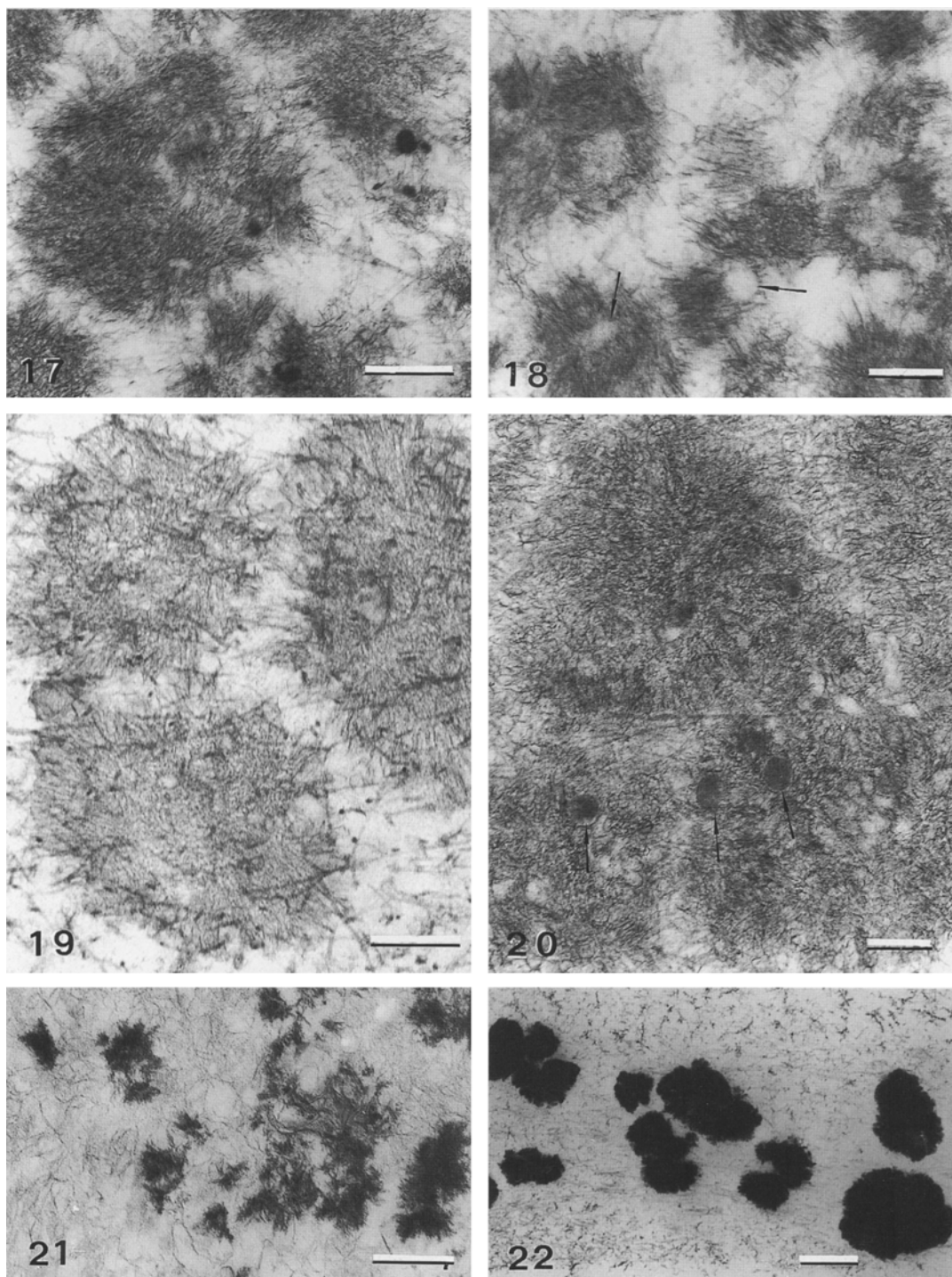


Fig. 17. Upper hypertrophic zone: detail of focal filament aggregates, only one of which is entirely visible; note that it is a roundish aggregate of thin filament-like structures whose ultrastructural morphology is similar to that described for apatite crystallites. U/Pb, $\times 15,500$; bar = 1 μm .

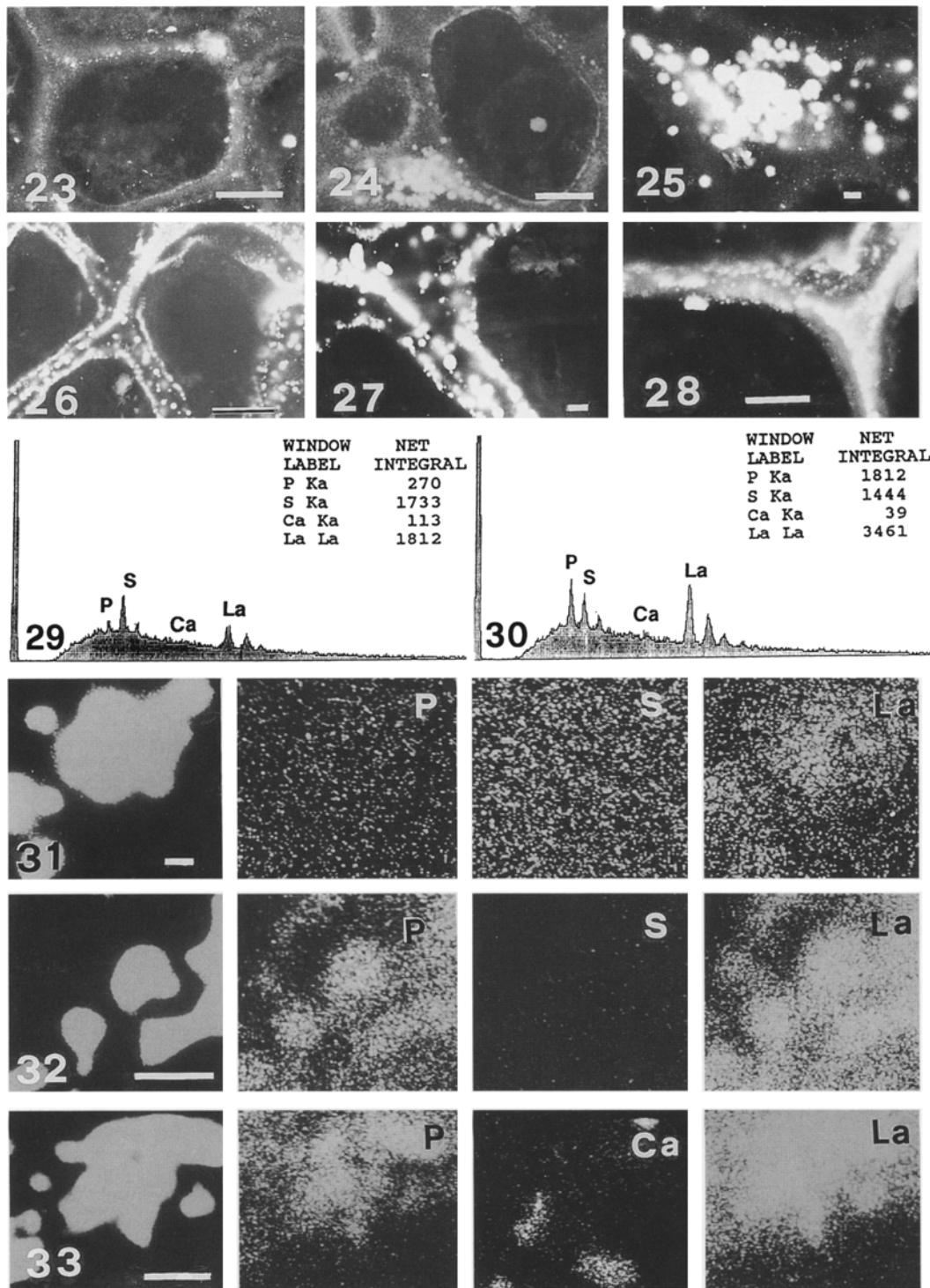
Fig. 18. Upper hypertrophic zone: light matrix vesicles (arrows) appear as empty vacuoles surrounded by a thin wall; they are associated with focal filament aggregates. U/Pb, $\times 28,500$; bar = 0.5 μm .

Fig. 19. Upper hypertrophic zone: three focal filament aggregates, one of which (upper right) is partly visible, are present in interterritorial matrix; their filaments are lightly stained by PTA, so that collagen fibrils irregularly crossing the aggregates are visible. PTA, $\times 15,500$; bar = 1 μm .

Fig. 20. Upper hypertrophic zone: dense matrix vesicles (arrows) are present within closely adjacent focal filament aggregates. PEDS method: formic acid-U/Pb, $\times 21,000$; bar = 0.5 μm .

Fig. 21. Lower hypertrophic zone: irregularly shaped deposits (i.e., irregular electron-dense deposits) are visible; they appear as very electron-dense, irregular clusters of badly visible filaments. Note that they are located over and among lightly stained filaments pertaining to focal filament aggregates. U/Pb, $\times 28,500$; bar = 0.5 μm .

Fig. 22. Lowest hypertrophic zone: only irregular electron-dense deposits are visible in this area; their high electron density masks the structures of the matrix, including the probably underlying focal filament aggregates. Note resemblance of these deposits with calcification nodules. U/Pb, $\times 8900$; bar = 2 μm .



free in the matrix (Fig. 14) and within roundish aggregates of filaments ("focal filament aggregates") (see below and Fig. 15). The dense MVs near the hypertrophic chondrocytes of the lowest zone were bigger than those of the upper zone, reaching 260–300 nm in diameter.

Another type of MV, devoid of electron-dense deposits and consequently called "light" MV, was present in the cartilage matrix. Because light MVs were frequently associated with focal filament aggregates, they are described below together with these structures.

The focal filament aggregates corresponded to the von Kossa-negative dots visible under the light microscope. They were small (0.2–1.3 μm in diameter), roundish, star-like, or irregular aggregates of thin filaments (about 2 nm thick) which were not visible in unstained sections, and were recognizable after staining with U/Pb (Figs. 14, 15, 16, 17, 18), PTA (Fig. 19), or PEDS method (Fig. 20). In PTA-stained sections they appeared irregularly crossed by collagen fibrils (Fig. 19). They were not visible in either unstained or stained sections of the control cartilage.

- Fig. 23.** Upper hypertrophic zone: correlated backscattered electron image (BSE) and SEM image: small and big deposits which produce BSE-signal are seen in the interterritorial matrix and at the border of the chondrocyte lacuna. A layer of unstained block surface is examined. $\times 2500$; bar = 10 μm .
- Fig. 24.** Upper hypertrophic zone: correlated BSE-SEM image of an area similar to that shown in Figure 6; clusters of deposits producing BSE-signal are present in the interterritorial matrix. A layer of unstained block surface is examined. $\times 1100$; bar = 10 μm .
- Fig. 25.** Upper hypertrophic zone: detail of the clusters of deposits (1–2 μm) shown in Figure 24; a layer of unstained block surface is examined. BSE-SEM, $\times 4300$; bar = 1 μm .
- Fig. 26.** Lower hypertrophic zone: correlated BSE-SEM image of an area similar to that shown in Figure 4: small deposits are present on the border of the chondrocyte lacuna and in the interterritorial matrix. A layer of unstained block surface is examined. $\times 1200$; bar = 10 μm .
- Fig. 27.** Lower hypertrophic zone: correlated BSE-SEM image of an area similar to that shown in Figure 9: small, globular deposits are present on the border of the chondrocyte lacuna, other bigger, irregular deposits are visible in the interterritorial matrix. A layer of unstained block surface is examined. $\times 4500$; bar = 1 μm .
- Fig. 28.** Lowest hypertrophic zone: correlated BSE-SEM image of an area similar to that shown in Figure 22: coalesced and fused deposits are visible on right. A layer of unstained block surface is examined. $\times 2700$; bar = 5 μm .
- Fig. 29.** Upper hypertrophic zone: X-ray microanalytical spectrum and net integral counts of P, S, Ca, and La obtained from the clusters of deposits that produce the BSE-signal. Scanned field = 10 \times 13 μm ; FS = 2K; time = 100 seconds.
- Fig. 30.** Lower hypertrophic zone: X-ray microanalytical spectrum and net integral counts of P, S, Ca, and La obtained from the irregular-shaped deposits that produce the BSE signal. Scanned field = 10 \times 13 μm ; FS = 2K; time = 100 seconds.
- Fig. 31.** Upper hypertrophic zone: computer display, backscattered electron image in conjunction with mapping X-ray microanalysis of P, S, and La of focal filament aggregates devoid of electron-dense deposits. SEM, $\times 11,000$, bar = 1 μm .
- Fig. 32.** Lower hypertrophic zone: computer display, backscattered electron image in conjunction with mapping X-ray microanalysis of P, S, and La of dense MVs and irregular-shaped electron-dense deposits. SEM, $\times 23,000$; bar = 1 μm .
- Fig. 33.** Lowest hypertrophic zone: computer display, backscattered electron image in conjunction with mapping X-ray microanalysis of P, Ca, and La of separated LaP-electron-dense deposits and Ca deposits in the interterritorial matrix. SEM, $\times 15,000$; bar = 1 μm .

The focal filament aggregates were first seen in the upper hypertrophic zone (Fig. 16), where they were in close relationship with light MVs (Fig. 18). These were electron-transparent, globular or ovoid (60–110 nm in diameter), membrane-bound structures that were found in association with focal filament aggregates (Fig. 18) and dense MVs (Figs. 14, 20). Light MVs were especially numerous in interterritorial matrix of the upper hypertrophic zone and were not found in either the territorial matrix or in association with the chondrocyte processes.

In the lower hypertrophic zone, the focal filament aggregates had reduced affinity for U/Pb (Fig. 21); moreover, they contained electron-dense deposits. Some of these deposits were dense MVs (Fig. 15), others corresponded to the second type of electron-dense deposits mentioned above (irregular electron-dense deposits) (Fig. 21). These consisted of aggregates of needle- and filament-like structures having a morphology similar to, and an electron density greater than, that of hydroxyapatite crystals (Fig. 11), so that they were visible in unstained sections. They also resembled U/Pb stained filaments of focal filament aggregates. These structures formed roundish and, more often, irregular aggregates and for this reason they are called "irregular electron-dense deposits."

The irregular electron-dense deposits were scattered throughout the interterritorial matrix of the lower hypertrophic zone and were located on the focal filament aggregates, which consequently were more or less completely masked (Figs. 21, 22). Especially in the lowest hypertrophic zone, the masking effect was often complete (Fig. 22), so that the deposits acquired a morphology similar to that of calcification nodules (i.e., early aggregates of inorganic crystals).

Correlated BSE-SEM in Conjunction with X-ray Microanalysis

The BSE-SEM provided high topographic contrast images of the La-incubated epiphyseal cartilage. The morphology of the chondrocytes was easily recognized; moreover, deposits that produced a BSE-signal were located in the interterritorial matrix and around chondrocytes of the hypertrophic cartilage. In the upper hypertrophic zone, the inter-

territorial deposits (1–2 μm in diameter) were disposed in clusters (Figs. 23, 24, 25). Other small deposits (about 0.1 μm thick) were seen around the chondrocyte peripheral membrane and in the interterritorial matrix (Figs. 23, 25). The BSE-signal deposits were more abundant in the lower hypertrophic zone (Fig. 26). Some of them were globular (about 0.1–0.2 μm in diameter) and were chiefly located around the chondrocyte peripheral membrane (Fig. 27), others were irregularly shaped and bigger (about 1–2 μm thick; Figs. 27, 28) and were located in the interterritorial matrix. In the lowest hypertrophic zone these deposits coalesced, forming plaques (Fig. 28).

The qualitative X-ray microanalysis study of the BSE-signal deposits showed different content of La, P, and S in them. In the upper hypertrophic zone the clusters of BSE-signal deposits found in the interterritorial matrix revealed spectral peaks of P, S, and La (Fig. 29). The P spectral peak was very low, and the X-ray count ratio La:P was 6:1. No Ca spectral peaks were detected. In the lower hypertrophic zone, the irregular-shaped deposits revealed peaks of P, S, and La (Fig. 30). The P and La spectral peaks were high, and the X-ray count ratio La:P was 2:1. No Ca spectral peaks were detected. The globular deposits at the peripheral membrane of the chondrocytes of the lower zone were composed of P and La spectral peaks, although a low S spectral peak was detected; no Ca spectral peaks were detected. The globular X-ray count ratio La:P was 2:1. The plaques found in the lowest hypertrophic zone revealed a spectrum composed of P, S, Ca, and La. Their X-ray count ratio Ca + La:P was 2:1. A silicon (Si) spectrum was detected in the single Ca deposits, but it was not found in the LaP deposits.

The X-ray mapping showed the peculiar distribution of the elements P, S, Ca, and La in the variety of BSE-signal deposits. In the upper hypertrophic zone, the X-ray mapping showed focal concentration of La over the clusters of BSE-signal deposits and a homogeneous distribution of S and P in them and in the surrounding matrix (Fig. 31). In the lower hypertrophic zone, the X-ray mapping showed a coincident distribution of P and La in the globular and irregular-shaped deposits (Fig. 32). In the lowest zones, the X-ray mapping showed La deposits and Ca deposits separately (Fig. 33). Thus, the BSE-signal detected was produced by La; and an exact correlation was found between BSE/X-ray mapping

images and light and electron microscope images. So in the upper hypertrophic zone the focal filament aggregates bound La but were devoid of LaP-electron-dense deposits. In the lower hypertrophic zone the focal filament aggregates and the dense matrix vesicles were loaded with LaP-electron-dense deposits. In the lowest zones LaP deposits and Ca deposits coexisted separately.

Discussion

After La incubation, the hypertrophic zone of the epiphyseal cartilage exhibited the same electron-dense deposits as the condylar cartilage [1]. As the electron-dense deposits appeared similar to apatite mineral, the X-ray microanalysis was necessary to confirm their La content [1]. In unstained cartilage, all electron-dense deposits were composed of P and La, with a constant X-ray count ratio La:P = 2:1; no Ca was demonstrable in them, except in lightly electron-dense deposits of the lowest hypertrophic zone. These findings, and especially the La:P ratio, would suggest that the La-P electron-dense deposits were in fact calcification nodules, and that the hydroxyapatite Ca had been substituted by La during the incubation period, with formation of La phosphate. However, because electron-dense La deposits of the hypertrophic cartilage are more abundant than calcification nodules, and because they are present in areas where no solid Ca phases are morphologically demonstrable, it may be thought that, rather than substituting for Ca, La binds to the same matrix sites that can potentially link Ca ions, thus simply "staining" Ca-binding sites.

The present findings seem to support the second possibility, but they do not solve the problem. If the electron-dense deposits were due to La substitution for Ca, they should contain silicon, as early apatite deposits do [4, 5]; on the contrary, silicon is not demonstrable. However, this element is described to be present in early solid, crystalline calcium phosphate deposits, whereas La-Ca substitution might occur in more labile, morphologically unrecognizable CaP phases such as amorphous calcium phosphate (ACP). This possibility is consistent with the recent observation that early MV mineralization is dependent on the presence of a labile, nucleational core of ACP [6, 7]. A second observation which seems to be against La substitution for Ca is that light microscopy, electron microscopy, and X-ray microanalysis show the coexistence of La and Ca deposits separately in the same microscopic field of the lowest hypertrophic zone. Again, it might be supposed that the La deposits are formed by La substitution for the Ca of labile deposits, whereas the Ca deposits correspond to a stable form of calcium salt that cannot be dismutated. A third observation which seems to be against La substitution is that no Ca deposits were recognizable in the upper and lower hypertrophic zones in control sections stained with the von Kossa method. However, this method is not very sensitive and probably does not reveal the earliest Ca deposits.

The X-ray count ratio La:P = 2:1 suggests that the electron-dense deposits correspond to a solid phase of La phosphate precipitated in precise sites during a period of incubation. While La³⁺ was supplied by incubation solution, the co-precipitation of phosphate remained of paramount importance to understand the nature of these sites, which can be considered the nucleation sites of a La phosphate (LaP) mineral.

The nucleation sites of LaP mineral were dual: dense matrix vesicles and focal filament aggregates. The dense MV is a specific type of MV which reveals an intrinsic capacity to precipitate intravesicular LaP mineral. This ca-

capacity, which is already present as soon as dense MVs bud from chondrocyte outer membrane, might depend on the presence in them of nucleational ACP core [6, 7]. The dense MVs might be those reported as having the property of both concentrating calcium ions and providing phosphate ions through the alkaline phosphatase activity [8]. However, in this case, the LaP stoichiometry would probably be variable, depending on the amounts of P liberated by AP; the ratio La:P = 2:1 suggests that Pi might derive directly from chondrocytes [9, 10]. In this regard, it has been shown that there are markedly elevated levels of [Ca²⁺]_{ic} in the cortical zone of the chondrocytes, and that this Ca is periodically exfoliated with MVs released from the chondrocytes into the matrix [11]. Because Pi is also involved in dynamic cellular metabolism, the MVs might have high concentration of both elements, so that after La incubation they might appear as dense MVs.

The light MVs are other MVs which seem to lack nucleating capacity. They were not seen in proximity of hypertrophic chondrocytes and were only present in interterritorial matrix. This suggests that they are formed either in the proliferative or maturative zones. The light MVs might correspond to MVs devoid of AP activity [12, 13]. Another possibility is that they do not react with La because they have lost their Ca and P ions. This possibility is suggested by results of Warner et al. [14] on ALP-rich MVs isolated by Percoll density-gradient fractionation from different regions of the growth cartilage: the MVs were separated into a low-density, noncalcifiable fraction (P-I fraction), and a high-density, readily calcifiable fraction (P-II fraction); during incubation in synthetic lymph to induce mineral formation, the P-II fraction separated into two ALP-rich fractions, one of increased density, another of the same low density as that of P-I fraction. The conclusion is that MVs are heterogeneous in functional capacities regarding mineral nucleation, and that the hypertrophic chondrocytes produce a specific type of mineralizing MV.

The second nucleation site described is the focal filament aggregate. The histochemical characteristics of these aggregates and their S content suggest that they are focal concentrations of proteoglycans. In this context, similar proteoglycan aggregates were found in the epiphyseal cartilage by chemical fixation with cationic dyes [15], and by cytochemical study using high-iron-diamine thiocarbonyl-silver-proteinase [16]. How the proteoglycans were focally concentrated is not known, but the proteolytic degradation of proteoglycans by a neutral protease [17], the presence in MVs of metalloproteinases [18], and the intimate relationship with light MVs depicted in this study suggest a link. On the other hand, the filament aggregates might have heterogeneous composition and, besides proteoglycans, they might contain other components such as phospholipids, the C-propeptide of type II collagen (chondrocalcin), type X collagen [19], and other substances. Concentration of chondrocalcin can be found in calcifying focal sites in the lower hypertrophic zone [19]; filamentous mats of type-X collagen can be found in cartilage matrix [20, 21]. Both chondrocalcin and type X collagen aggregates resemble focal filament aggregates; both are Ca-binding proteins [19, 22]. Type X collagen also binds to MVs [23, 24] and link protein and hyaluronic acid-binding region of proteoglycans that are also bound to MVs [25]. These findings suggest that the focal filament aggregates might contain not only proteoglycans, but also chondrocalcin and type-X collagen. Obviously, the simple morphological similarity of these structures does not resolve the question of the nature of the filaments.

The appearance of LaP mineral deposits within the focal

filament aggregates requires two steps. Before precipitation of LaP mineral, a focal concentration of La is contained in these structures in the upper hypertrophic zone where they are first seen. The La was not detected in "unstained" ultrathin sections, but correlated studies on the "unstained" flat block surface with BSE-SEM showed a "cloud" BSE signal in the same position as that of La deposits in stained sections. X-ray microanalysis confirmed that the BSE signal originates from La. The acquisition of La-binding capacities by the focal filament aggregates may reflect the calcium-binding properties attributed to focal concentrations of proteoglycans [19, 26]. How the complex La focal filament aggregates precipitate LaP mineral is not known. The ultrastructural findings suggest the participation of "crystal ghosts" as in early calcification sites [27–29]. The organic filamentous structures which constitute the focal filament aggregates might be the equivalent of the Ca-binding crystal ghosts found in calcification nodules of cartilage [28–30]. It is of interest that both the crystal ghosts and the filaments of the focal aggregates correspond to acid proteoglycans [28–30].

With regard to the supply of phosphate ions, biochemical studies correlated with X-ray microanalysis and histological studies, show that the hypertrophic cartilage contains large amounts of organic and high AP activity [31]. So it is possible that the P which co-precipitated with La within the focal filament aggregate is provided by the AP activity from native organic P substrates during the incubation period. In this context, the Ca²⁺-binding glycoprotein AP has been detected by cytochemical and immunocytochemical methods in early cartilage calcification sites [8, 32]; moreover, this AP interacts *in vitro* with proteoglycan subunits in epiphyseal cartilage [33]. Therefore, the coupled actions of La binding to focal concentrations of proteoglycans and phosphate production by AP activity might be necessary for the nucleation of LaP mineral. However, the development of LaP deposits from MVs cannot be excluded: no serial sections were made to discover the presence of MVs in the proximity of the deposits.

After initial appearance of LaP mineral within the focal filament aggregates and dense matrix vesicles, a bulk phase seems to ensue from the different nuclei. The bulk phase was evident in the lowest hypertrophic zone, where the territorial and interterritorial matrices were almost completely filled with LaP mineral deposits. The existence of dense MVs within the focal filament aggregates suggests that dense MVs provided extra nuclei.

In conclusion, the descriptive ultrastructural and X-ray microanalytical study suggests that, before the beginning of the calcification process, the La incubation method detects the matrix Ca binding components (which link La ions) and the matrix calcification initiation sites (which cause focal precipitation of LaP mineral).

Acknowledgments. This investigation is part of the cooperative project between the University of Rome La Sapienza (Italy) and the University of Cadiz (Spain); supported by grants from the University of Cadiz and Roma La Sapienza, the Italian National Research Council, and the Italian Ministry of University and Scientific and Technological Research (MURST).

References

- Morris DC, Appleton J (1984) The effects of lanthanum on the ultrastructure of hypertrophic chondrocytes and the localization of lanthanum precipitates in condylar cartilages of rats fed on normal and rachitogenic diets. *J Histochem Cytochem* 32: 239–247
- Bonucci E, Reurink J (1978) The fine structure of decalcified cartilage and bone: a comparison between decalcification procedures performed before and after embedding. *Calcif Tissue Res* 25:179–190
- Gomez S, Boyde A (1994) Correlated alkaline phosphatase histochemistry and quantitative backscattered electron imaging in the study of rat incisor ameloblasts and enamel mineralization. *Microsc Res Technique* 29:29–36
- Arsenault AL, Hunziker EB (1988) Electron microscopic analysis of mineral deposits in the calcifying epiphyseal growth plate. *Calcif Tissue Int* 42:119–126
- Landis WJ, Glimcher MJ (1982) Electron optical and analytical observations of rat growth plate cartilage prepared by ultracytometry: the failure to detect a mineral phase in matrix vesicles and the identification of heterodispersed particles as the initial solid phase of calcium phosphate deposited in the extracellular matrix. *J Ultrastruct Res* 78:227–268
- Wu LNY, Yoshimori T, Genge BR, Sauer GR, Kirsch T, Ishikawa Y, Wuthier RE (1993) Characterization of the nucleational core complex responsible for mineral induction by growth plate cartilage matrix vesicles. *J Biol Chem* 268: 25084–25094
- Kirsch T, Ishikawa Y, Mwale F, Wuthier RE (1994) Roles of the nucleational core complex and collagens (types II and X) in calcification of growth plate cartilage matrix vesicles. *J Biol Chem* 269:20103–20109
- Sela J, Schwartz Z, Swain LD, Boyan BD (1992) The role of matrix vesicles in calcification. In: Bonucci E (ed) *Calcification in biological systems*. CRC Press, Boca Raton, pp. 73–105
- Wuthier RE (1977) Electrolytes of isolated epiphyseal chondrocytes, matrix vesicles, and extracellular fluid. *Calcif Tissue Res* 23:125–133
- Pollesello P, de Bernard B, Grandolfo M, Paoletti S, Vittor F, Kvam BJ (1991) Energy state of chondrocytes assessed by ³¹P-NMR studies of preosseous cartilage. *Biochem Biophys Res Comm* 180:216–222
- Wuthier RE (1992) Matrix vesicles: formation and function. Mechanisms in membrane/matrix-mediated mineralization. In: Slavkin H, Price P (eds) *Chemistry and biology of mineralized tissues*. Excerpta Medica, Amsterdam, pp 143–152
- Bonucci E, Silvestrini G, Bianco P (1992) Extracellular alkaline phosphatase activity in mineralizing matrices of cartilage and bone: ultrastructural localization using a cerium-based method. *Histochemistry* 97:323–327
- Lewinson D, Toister Z, Silbermann M (1982) Quantitative and distributional changes in the activity of alkaline phosphatase during the maturation of cartilage. *J Histochem Cytochem* 32:261–269
- Warner GP, Hubbard HL, Lloyd GC, Wuthier RE (1983) ³²Pi- and ⁴⁵Ca-metabolism by matrix vesicle-enriched microsomes prepared from chicken epiphyseal cartilage by isosmotic Percoll density-gradient fractionation. *Calcif Tissue Int* 35: 327–338
- Shepard N (1992) Role of proteoglycans in calcification. In: Bonucci E (ed) *Calcification in biological systems*. CRC Press, Boca Raton, pp 41–58
- Takagi M (1990) Ultrastructural cytochemistry of cartilage proteoglycans and their relation to the calcification process. In: Bonucci E, Motta PM (eds) *Ultrastructure of skeletal tissues*. Kluwer Academic Publishers, Boston, pp 111–127
- Ehrlich MG, Armstrong AL, Neuman RG, Davis MW, Mankin HJ (1982) Patterns of proteoglycan degradation by a neutral protease from human growth-plate epiphyseal cartilage. *J Bone Joint Surg Am* 64:1350–1354
- Dean DD, Schwartz Z, Muniz OE, Gomez R, Swain LD, Howell DS, Boyan BD (1992) Matrix vesicles are enriched in metalloproteinases that degrade proteoglycans. *Calcif Tissue Int* 50:342–349
- Poole R, Matsui Y, Hinek A, Lee ER (1989) Cartilage macromolecules and the calcification of cartilage and bone. *Anat Rec* 224:167–179
- Schmid TM, Linsenmayer TF (1990) Immunoelectron micros-

- copy of type X collagen: supramolecular forms within embryonic chick cartilage. *Dev Biol* 138:53–62
21. Kwan APL, Cummings CE, Chapman JA, Grant ME (1991) Macromolecular organization of chicken type V collagen in vitro. *J Cell Biol* 114:597–604
 22. Kirsch T, von der Mark K (1991) Ca²⁺ binding properties of type X collagen. *FEBS Lett* 294:149–152
 23. Wu LNY, Genge BR, Lloyd GC, Wuthier RE (1991) Collagen-binding proteins in collagenase-released matrix vesicles from cartilage. *J Biol Chem* 266:1195–1203
 24. Kirsch T, Wuthier RE (1994) Stimulation of calcification of growth plate cartilage matrix vesicles by binding to type II and X collagens. *J Biol Chem* 269:11462–11469
 25. Wu LNY, Genge BR, Wuthier RE (1991) Association between proteoglycans and matrix vesicles in the extracellular matrix of growth plate cartilage. *J Biol Chem* 266:1187–1194
 26. Poole AR (1991) The growth plate: cellular physiology, cartilage assembly and mineralization. In: Hall B, Newman S (eds) *Cartilage: molecular aspects*. CRC Press, Boca Raton, pp 179–211
 27. Bonucci E (1967) Fine structure of early cartilage calcification. *J Ultrastruc Res* 20:33–50
 28. Bonucci E, Silvestrini G (1992) Immunohistochemical investigation on the presence of chondroitin sulfate in calcification nodules of epiphyseal cartilage. *Eur J Histochem* 36:407–422
 29. Bonucci E, Silvestrini G, Di Grezia R (1988) The ultrastructure of the organic phase associated with the inorganic substance in calcified tissues. *Clin Orthop Rel Res* 233:243–261
 30. Bonucci E, Silvestrini G, Di Grezia R (1988) Histochemical properties of the “crystal ghosts” of calcifying epiphyseal cartilage. *Connect Tissue Res* 22:43–50
 31. Althoff J, Quint P, Krefting E-R, Höhling HJ (1982) Morphological studies on the epiphyseal growth plate combined with biochemical and X-ray microprobe analyses. *Histochemistry* 74:541–552
 32. de Bernard B, Bianco P, Bonucci E, Costantini M, Lunazzi GC, Martinuzzi P, Modricky C, Moro L, Panfili E, Pollesello P, Stagni N, Vittur F (1986) Biochemical and immunohistochemical evidence that in cartilage an alkaline phosphatase is a Ca²⁺-binding glycoprotein. *J Cell Biol* 103:1615–1623
 33. Vittur F, Stagni N, Moro L, de Bernard B (1984) Alkaline phosphatase binds to collagen: a hypothesis on the mechanism of extravesicular mineralization in epiphyseal cartilage. *Experientia* 40:836–837